Plant Physiology and Biochemistry 144 (2019) 92–99

Contents lists available at ScienceDirect

Plant Physiology and Biochemistry

journal homepage: www.elsevier.com/locate/plaphy

Research article

Unbiased phosphoproteome profiling uncovers novel phosphoproteins and phosphorylation motifs in bermudagrass stolons

Bing Zhang[a,*], Jingbo Chen[b], Junqin Zong[b], Xuebing Yan[a], Jianxiu Liu[b]

[a] College of Animal Science and Technology, Yangzhou University, Yangzhou, 225009, China
[b] Institute of Botany, Jiangsu Province and Chinese Academy of Sciences, Nanjing, 210014, China

ARTICLE INFO

Keywords:
Bermudagrass
Cynodon dactylon
Phosphorylation
Starch
Stolon
Phosphoproteome

ABSTRACT

As a widely used turfgrass species, bermudagrass (*Cynodon dactylon* L.) can be easily propagated through colonial growth of stolons. Previous studies collectively revealed that exotic environmental factors and intrinsic hormones and genes are all involved in the differentiation, development, and diageotropical growth of stolons. However, the detailed molecular mechanism how environmental and hormone signals regulate the gene expression and biochemical activities in bermudagrass stolons remains unclear. In this study, we observed that reversible phosphorylation modification plays important roles in normal growth and physiological functions of bermudagrass stolons. LC-MS/MS analyses of the total protein extracts of bermudagrass stolons without preliminary phosphopeptide-enrichment successfully identified 646 nonredundant phosphorylation sites and 485 phosphoproteins. The phosphoproteins were significantly enriched in protein phosphorylation regulation and starch metabolism processes. Motif-X analyses further revealed that phosphoproteins containing novel phosphorylation motifs might be involved in transcription regulation of bermudagrass stolons. These results greatly expanded our understanding of the growth and development of bermudagrass stolons at the post-translational level.

1. Introduction

As an important perennial warm-season turfgrass species, bermudagrass (*Cynodon dactylon* L.) is widely used to produce high-quality turf for home lawns, public parks, sport fields and golf courses in tropical and subtropical regions (Chen et al., 2017; Munshaw et al., 2004). Unlike cool-season turfgrasses including ryegrass and tall fescue, bermudagrass has well-developed prostrate-growing stems, stolons, which enable it to fast propagate and tolerant to stresses, especially the wear stress (Dunne et al., 2019; Lulli et al., 2011). Elucidating the mechanism how bermudagrass stolons differentiate, develop and grow diageotropically could not only expand our understanding of plant architecture formation and regulation but also help us to breed new turfgrass cultivars with superior turf quality.

Light, gravity and phytohormones, including auxin, ethylene and gibberellin, are all involved in the differentiation and prostrate growth of bermudagrass stolons (Balatti and Willemöes, 1989; Willemoës et al., 1987). Notably, shading treatment, by modulating the ratio of red/far red light, could inhibit the differentiation of stolons through phytochrome-mediated photoassimilate partitioning (Beltrano et al., 1991; Guglielmini and Satorre, 2002). Low sucrose levels could also promote erect growth of stolons, which behaved resembling the growth mode of shoots (Montaldi, 1969). High-throughput comparative transcriptomics analyses of two bermudagrass wild accessions with different stolon/shoot ratios indicated that numerous genes are possibly related to shoot and stolon differentiation and specialization (Zhang et al., 2017). However, the detailed molecular mechanism how these genes and their encoding protein products synergically respond to environmental and phytohormone signals to coordinate the cellular processes required for stolon growth and development are still uncharacterized.

Reversible phosphorylation is the most widespread protein modification affecting nearly all cellular processes including signal transduction, gene expression, cell cycle progression and metabolic reactions (Needham et al., 2019; Silva-Sanchez et al., 2015). In the past several years, many studies have elucidated the important regulatory functions of protein phosphorylation in maintaining a plastic plant architecture (Wu et al., 2018). For example, shade-induced dephosphorylation of phytochrome-interacting factor 7, a basic helix-loop-helix (bHLH) transcription factor, increase its transactivation activity to promote auxin synthesis in Arabidopsis, which is required for the rapid plant architecture change to adapt the light-deficient environment (Li et al., 2012). In *Mimosa pudica*, tyrosine phosphorylation of actin is essential for fast petiole bending in response to touch (Kameyama et al., 2000). In maize, mitogen-activated protein kinase-regulated protein

* Corresponding author.
E-mail address: bingzhang@yzu.edu.cn (B. Zhang).

https://doi.org/10.1016/j.plaphy.2019.09.036
Received 5 June 2019; Received in revised form 6 September 2019; Accepted 21 September 2019
Available online 22 September 2019
0981-9428/

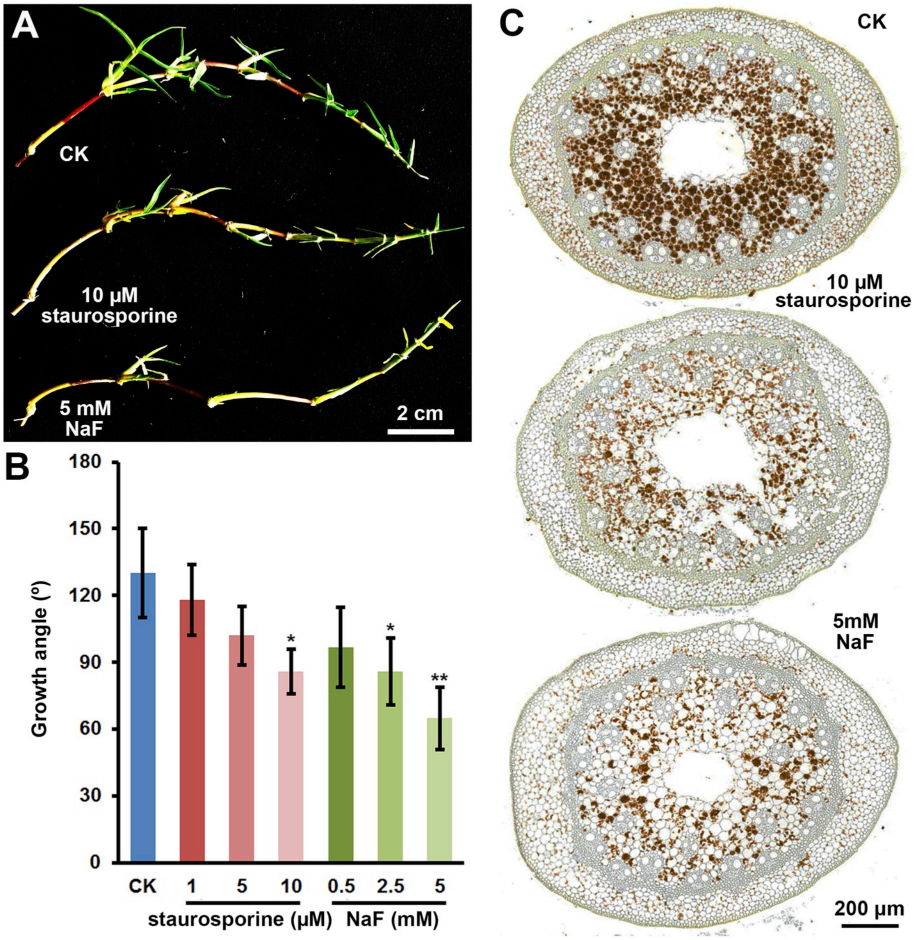

Fig. 1. Phenotypes of bermudagrass stolons under protein kinase and phosphatase inhibitor treatments. A) Stolons of bermudagrass cultivar Yangjiang growing in Hoagland's nutrient solution without (CK) and with 10 μM staurosporine or 5 mM NaF treatments for 24 h. B) Growth angle of the stolon terminal 2nd internodes without (CK) and with different concentrations of staurosporine or NaF treatments for 24 h. Asterisks indicate significant differences determined by Student's t-tests (*, $p < 0.05$, **, $p < 0.01$). C) I_2-KI staining for starch accumulation in the stolon terminal 2nd internodes without (CK) and with staurosporine or NaF treatments.

phosphorylation is involved in gravity sensing and response (Clore et al., 2003). However, whether these phosphorylation-dependent regulatory mechanisms are involved in stolon differentiation and development in bermudagrass, remains unclear.

More recently, the improvement of high-resolution mass spectrometric instruments have facilitated the large-scale comprehensive analysis of protein phosphorylation in many plant species, including Arabidopsis, rice, maize, soybean, spinach, kiwifruit, wheat, *Medicago truncatula* and *Brachypodium distachyon* (Chao et al., 2016; Liñeiro et al., 2016; Lu et al., 2008; Lv et al., 2014; Meyer et al., 2012; Nakagami et al., 2010; Pan et al., 2018; Rose et al., 2012; Vannini et al., 2019; Yuan et al., 2016; Zhao et al., 2018; Zhang et al., 2014). Results of these phosphoproteomics studies provided many new insights into the plant growth, development, and stress responses. In this study, we identified 692 phosphopeptides and 485 phosphoproteins from bermudagrass stolons without preliminary phosphopeptide-enrichment. Analyses of the phosphoproteins successfully revealed significantly phosphorylation-regulated biological processes and novel phosphorylation motifs in bermudagrass stolons. These results greatly improved our understanding of the phosphorylation-dependent regulation of stolon growth and development in bermudagrass.

2. Materials and methods

2.1. Plant material

C. dactylon cultivar Yangjiang was used in this study. The cultivar was grown at the turfgrass plots of the Nanjing Botanical Garden (32°02′N, 118°28′E; 30 m a.s.l.; average maximum/minimum temperatures: 38.1 °C/-5.7 °C; average annual precipitation: 1106 mm; soil type: 80% river sand mixed with 20% peat soil) under standard management conditions as previously described (Zhang and Liu, 2018).

2.2. Inhibitor treatment and curvature measurements

The third stolon nodes of *C. dactylon* cultivar Yangjiang were cut from the plants, fixed in a floating foam board and transferred to the Hoagland's nutrient solution as previously described (Chen et al., 2014). The node-originated new *C. dactylon* seedlings were grown in a growth chamber at 28 °C with a photoperiod of 16 h/8 h of white light for 2 weeks. The new *C. dactylon* plants with uniform stolons were then transferred to the Hoagland's nutrient solution without (CK) and with different concentrations of staurosporine or NaF. For each treatments, five plants were used as biological replicates. After 24 h, the growth angle of terminal 2nd internodes of stolons from each plants were measured using an angle gage. Student's t-test was used to determine the significant differences between CK and treatments.

2.3. Starch staining

After measurement of growth angle, the middle portions of the terminal 2nd internodes of stolons were harvested and immersed in FAA fixation buffer for 24 h. After dehydration in an ethanol series (60, 70, 85 and 95%), the internodes were embedded in paraffin. Tissue sections (15 μm thick) were cut with a Leica VT 1000S vibrotome (Leica, Nussloch, Germany) and mounted on glass slides. The slides were stained with KI-I_2 solution (1% KI and 0.3% I_2) (Wang et al., 1994). The sections were observed and photographed using an Olympus BX51T microscope (Olympus, Tokyo, Japan).

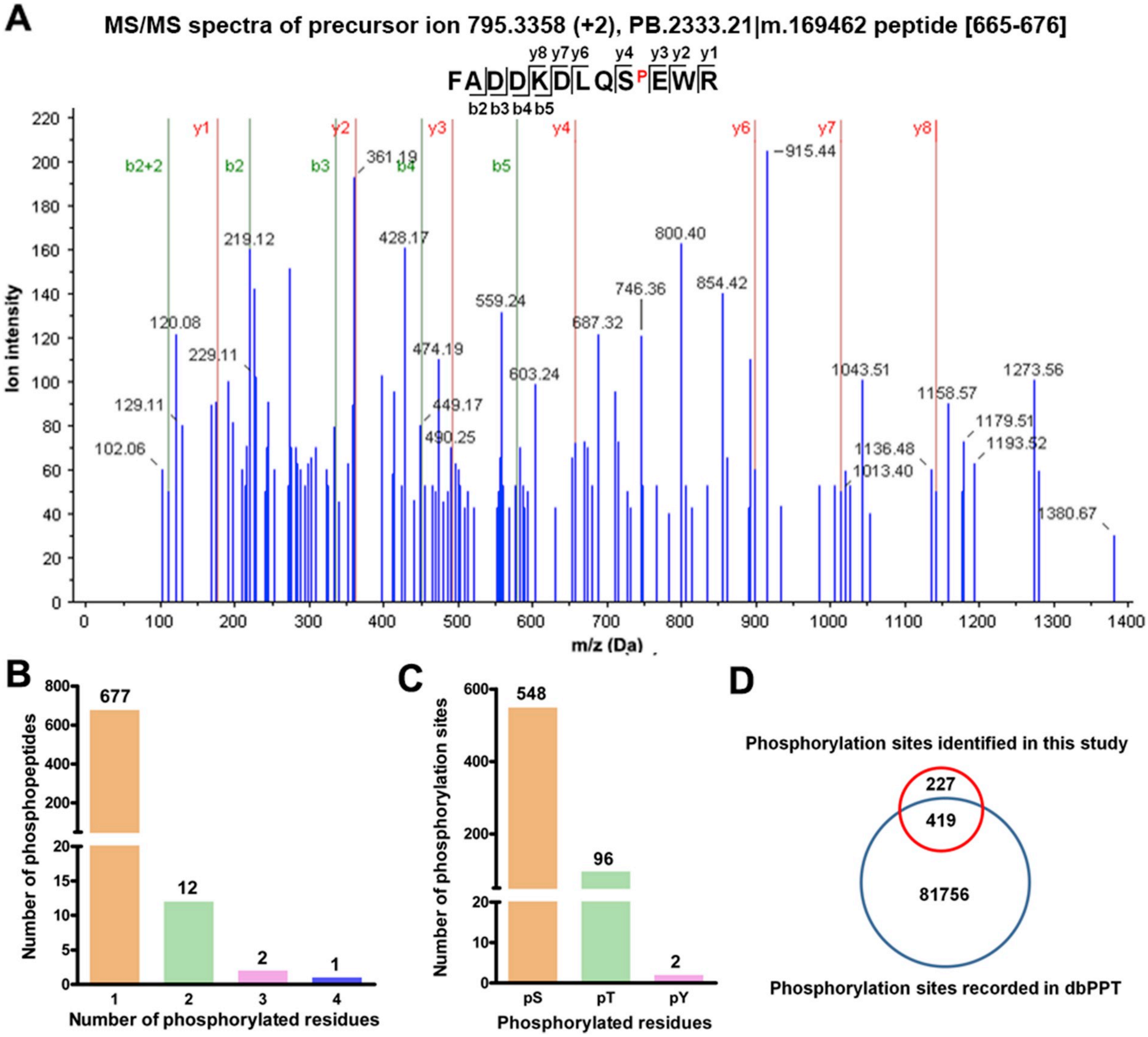

Fig. 2. Analyses of the identified phosphorylation sites in bermudagrass stolons. A) MS/MS spectra of one representative phosphopeptide FADDKDLQSPEWR identified in this study. B) Distribution of phosphopeptides containing different number of phosphorylated residues. C) Distribution of phosphorylated amino acids. D) Venn diagram analysis of the phosphorylation sites identified in this study and phosphorylation sites recorded in dbPPT database.

2.4. Protein extraction

Proteins were extracted from fresh stolons collected from different plants of *C. dactylon* cultivar Yangjiang using the previously described method with minor modifications (Yao et al., 2006). Briefly, about 0.5 g sample was ground in liquid nitrogen to a fine powder, and the powder was suspended completely in 10 ml of lysis buffer (7 M urea, 2 M Thiourea, 4% SDS, 40 mM Tris-HCl, pH 8.5, 10 mM DTT, 2 mM EDTA, 1 mM PMSF, 100 × protease inhibitor cocktail (P2714; Sigma, Shanghai, China), and 100 × phosphate inhibitor cocktails I and II (Sigma; P2850 and P5726, respectively)) with sonication on ice. The homogenate was centrifuged at 14,000 g for 30 min at 4 °C to remove the remaining debris. Subsequently, 4 volume of ice-cold acetone was added and the proteins were precipitated overnight at −20 °C. After centrifugation at 14,000 g for 30 min at 4 °C, the precipitate was collected and washed with ice-cold acetone for three times. The collected protein pellets were dried with N_2 to remove any remaining acetone. The dried protein powder was resuspended completely in 1 ml of dissolvent buffer (8 M urea, 100 mM TEAB, pH 8.0). The protein concentration was determined using Bradford method (Bradford, 1976).

2.5. Western blotting assay of protein phosphorylation

For western blotting assays, 20 μg of extracted protein samples were denatured in 6 × SDS/PAGE sampling buffer by boiling at 100 °C for 5 min, separated by 12% SDS/PAGE and transferred to a PVDF membrane. The first and secondary antibodies used were pan-phosphorylation antibody (ab15556; Abcam, Cambridge, USA) and goat anti-mouse antibody conjugated to horseradish peroxidase (A16078; Thermo Scientific, Waltham, USA). The signals were developed with a Lumilight western blotting substrate (Roche, Mannheim, Germany). The experiments were repeated three times using different stolon protein samples.

2.6. Trypsin digestion, desalting and fraction

Before tryptic digest, the protein sample was firstly reduced with 10 mM DTT for 45 min at 50 °C and alkylated with 50 mM iodoacetamide for 45 min at room temperature in the dark. For trypsin digestion, 100 μg protein was diluted by four volume of digestion buffer (100 mM TEAB, pH 8.0) and 2 μg of Trypsin Gold (Promega, Madison, USA) was added and incubated overnight at 37 °C. The digested peptides were desalted using a Strata-X C18 SPE column, dried by vacuum

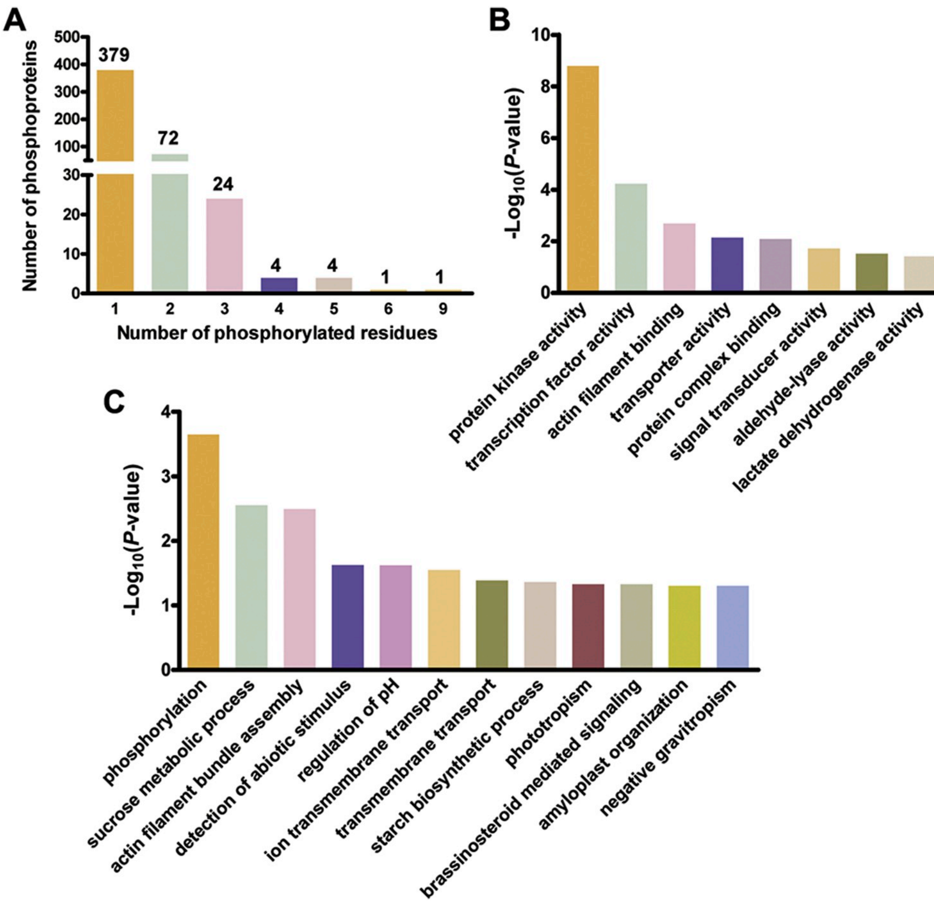

Fig. 3. Analyses of the identified phosphoproteins in bermudagrass stolons. A) Distribution of phosphoproteins containing different number of phosphorylated residues. B) Molecular functions significantly enriched with phosphoproteins. C) Biological processes significantly enriched with phosphoproteins.

centrifugation and fractionated using an Ultimate 3000 HPLC system (Dionex, Sunnyvale, USA) with Durashell C18 column (250 mm × 4.6 mm, 5 μm, 100 Å). Briefly, peptides were first fractionated with a gradient of 2%–60% acetonitrile in ammonium bicarbonate (10 mM, pH 10) over 60 min into 30 fractions, which were further combined into 6 final fractions and then desalted and vacuum dried.

2.7. Liquid chromatography-tandem mass spectrometry (LC-MS/MS) analysis

For LC-MS/MS analyses, the fractionated peptides were dissolved in solvent A (0.1% formic acid in 3% acetonitrile, 97% H_2O), loaded onto a reversed-phase pre-column (20 mm × 100 μm, 5 μm) and separated using a reversed-phase analytical column (150 mm × 75 μm, 3 μm) through the Eksigent nanoLC system (Eksigent, Livermore, USA). The gradient for MS analysis was set as the following: starting from 7% to 20% solvent B (0.1% formic acid in 97% acetonitrile, 3% H_2O) over 24 min, then 20%–35% solvent B in 8 min, thereafter increasing to 80% solvent B in 55 min and holding at 80% solvent B for the last 3 min, with a flow rate of 200 nL/min. MS data of three different stolon protein samples were collected using information-dependent acquisition mode in a high speed TripleTOF™ 5600plus mass spectrometer (ABSciex, Concord, Canada) coupled with the Eksigent nanoLC system. Briefly, the mass spectrometer was operated in a manner that a 0.25 s survey scan (MS) in the mass range of 350–1500 m/z was collected, from which the top 30 ions were selected for automated MS/MS in the mass range of 100–1500 m/z and each MS/MS event consisted of a 0.05 s scan. Once a target ion had been fragmented by MS/MS, its mass and isotopes were excluded for a period of 15 s.

2.8. Library searching and peptide identification

Analyses of the raw MS spectra generated by LC-MS/MS were performed with the ProteinPilot™ 4.5 software (ABSciex) using the Paragon algorithm and Andromeda integrated in MaxQuant 1.6.7.0 (Tyanova et al., 2016; Wang et al., 2016). Specifically, the false discovery rate (FDR) threshold was set at 0.01 and a high-confident peptide database (210,172 sequences, 69,486,195 residues) derived from a full-length transcriptome sequencing project of bermudagrass was used as the searching database (Zhang et al., 2018). The ProteinPilot-based searches were performed using the following settings: type of search, identification; enzyme, trypsin; Cys alkylation, iodoacetamide; special factors, phosphorylation emphasis; instrument, TripleTOF™ 5600plus; bias correction, true; background correction, true; ID focus, biological modifications; search effort, thorough ID; protein mass, unrestricted; unused score, ≥ 1.3; confidence, ≥ 95%; unique peptides, ≥ 1. The MaxQuant-based searches were performed using the default settings (MS/MS match tolerance, 20 ppm; minimum peptide length, 7; minimum score for modified peptides (PTMscore), 40) with oxidation of methionine and phosphorylation of serine, threonine and tyrosine residues were set as variable modifications. Peptides that were reproducibly identified in all three biological replicates using both two search engines were considered as valid identification and used for the further analysis. The identified phosphopeptides were further analyzed by LuciPHOr2 (MS/MS tolerance, 20 ppm; PeptideProphet probability, 0.95) to assign the most possible phosphorylation site location with a false localization rate (FLR) threshold of 0.01 (Fermin et al., 2015).

Table 1
Protein kinases and phosphatases identified with phosphorylation modifications in bermudagrass stolons.

Accession No.	Protein Name	Phosphopeptide
Protein kinase		
PB.48,998.7	serine/threonine-protein kinase SAPK7	S^{P}TVGTPAYIAPEVLSR
		AVHAS^{P}GDFQHLIK
PB.15,756.3	serine/threonine-protein kinase BLUS1	GIS^{P}GWNFNLEDLK
		SAS^{P}VPLNLDSSR
		ARNT^{P}FVGTPCWMAPEVMQQLHGYDYK
PB.1077.3	SNF1-related protein kinase regulatory subunit gamma-1	VEDLWEVAQPQLS^{P}PSEK
		AGS^{P}PVGSPVANIAAR
PB.8363.5	sucrose nonfermenting 4-like protein	TVS^{P}LSDGALQEGHQR
PB.8624.19	probable LRR receptor-like serine/threonine-protein kinase At1g56130	SAAAQNS^{P}SPFLSSVIDEGR
PB.2598.7	Protein kinase protein with octicosapeptide/Phox/Bem1p domain	DFPIS^{P}PSSAR
		YGEVDSPWS^{P}PAYVSPSQYGVHDPR
PB.877.4	calcium-dependent protein kinase 2	DIVGS^{P}AYYVAPEVLR
PB.4765.7	putative serine/threonine-protein kinase dyrk2	S^{P}IGVGISSDAADIGSEVR
		VIDLGSSCFETDHLCS^{P}YVQSR
PB.45,075.1	serine/threonine protein kinase OSK1	TS^{P}CGSPNYAAPEVISGK
		DGHFLKT^{P}SCGSPNYAAPEVISGK
PB.17,572.7	serine/threonine-protein kinase tricorner	MLAYS^{P}TVGTPDYIAPEVLLK
PB.57,607.7	mitogen-activated protein kinase kinase 1	GQDTPVDKFLTASGT^{P}FKDGELR
PB.4690.3	probable serine/threonine protein kinase IREH1	VSNSSINEESDGPS^{P}PK
PB.44,735.2	probable serine/threonine-protein kinase At4g35230	DGKSYS^{P}TNLAYTPPEYLR
PB.32,069.1	cysteine-rich receptor-like protein kinase 6	VRS^{P}YTETSELVR
		VRS^{P}YTETSELVREELCSESQSSITELYPR
PB.40,591.8	serine/threonine-protein kinase HT1-like	SGS^{P}LGSKDTYLR
PB.11,070.3	serine/threonine-protein kinase EDR1	SIS^{P}ITPEIGDDIVR
PB.921.33	serine/threonine-protein kinase STE20 isoform X1	TAS^{P}FGELLR
PB.6741.1	serine/threonine-protein kinase fray2 isoform X2	GVS^{P}AWNFDIEDLK
PB.5712.6	Cyclin-dependent kinase G-2	VAAMAPSAGASVSS^{P}PSK
PB.26,970.4	probable LIM domain-containing serine/threonine-protein kinase	SAS^{P}LTALSQAPR
PB.50,289.5	putative serine/threonine-protein kinase Cx32, chloroplastic	S^{P}TTGGFDEGSKSPLGQILEAPNLR
PB.53,393.1	SNF1-related protein kinase regulatory subunit gamma-1	AGS^{P}PVGSPVADIAAR
PB.36,017.7	serine/threonine protein kinase OSK4 isoform X2	LADFGLSNVMHDGHFLKTS^{P}CGSPNYAAPEVISGR
PB.38,122.2	serine/threonine-protein kinase STY46	FQDQGGIMT^{P}AETGTYR
PB.4585.9	CBL-interacting protein kinase 11-like	RQDGLLHT^{P}TCGTPAYVAPEVLSR
PB.9921.1	Serine/threonine-protein kinase CTR1	LCADAASAADPGFLDPGESGSGS^{P}GR
PB.31,703.4	serine/threonine-protein kinase AtPK2/AtPK19-like	SNS^{P}MCGTLEYMAPEILLGR
PB.18,883.7	casein kinase 1-like protein 3 isoform X1	VGAS^{P}PDNALLQSTSLGR
PB.36,549.5	probable receptor-like protein kinase At2g42960	TKSS^{P}DADNLSQCSSAYQLDR
PB.183.3	1-phosphatidylinositol-3-phosphate 5-kinase FAB1B	RVVS^{P}DGQFPVTADIPDTLDTK
Protein phosphatase		
PB.54,927.3	probable protein phosphatase 2C 54	SIS^{P}ADGLNSLR
PB.22,240.12	serine/threonine protein phosphatase 2A 57 kDa regulatory subunit B	DLAGAGSSLPS^{P}PTSDAR
PB.43,808.2	putative protein phosphatase 2C 64	VNS^{P}LVQLPR
PB.4940.1	serine/threonine-protein phosphatase BSL2 homolog isoform X2	QLS^{P}IDQFENEGR
		QMS^{P}INSVPK
		LIHPLPPAITSPETS^{P}PDHIEDTWMQELNANRPPTPTR
PB.12,291.5	serine/threonine-protein phosphatase BSL1 homolog isoform X2	QLS^{P}LDQFENESR

2.9. Bioinformatics analyses

The identified phosphoproteins were BLAST searched against the dbPPT dataset (http://dbppt.biocuckoo.org/index.php) with parameters set at an p-value < 0.01 to obtain the most homologous phosphorylation sites previously identified in plants (Cheng et al., 2014). The amino acid sequences of all the identified proteins were subjected to BLAST searches using the Ami Gene Ontology (GO) database (http://amigo1.geneontology.org/cgi-bin/amigo/blast.cgi) (Carbon et al., 2009). The corresponding GO terms were extracted from the most homologous proteins using a Perl program. The GO term distribution of phosphoproteins was statistically compared with that of all the identified proteins using Fisher's exact test with parameters set at an FDR-corrected p-value < 0.01 to obtain the significantly phosphoprotein-enriched GO terms. To predict conserved phosphorylation motifs, peptides of 15 amino acid in length with phosphorylated residues in the center were searched against all the identified proteins in Motif-X online search engine (http://motif-x.med.harvard.edu/) (Schwartz and Gygi, 2005). The occurrence threshold was set at 20 and the p-value threshold was set at $< 10^{-6}$.

2.10. Accession numbers

The mass spectrometry proteomics data have been deposited to the ProteomeXchange Consortium via the PRIDE partner repository with the dataset identifier PXD014113.

3. Results and discussion

3.1. Importance of reversible protein phosphorylation in bermudagrass stolons

Under normal growth conditions, stolons of bermudagrass showed downward growth (Fig. 1A). Addition of 1 μM staurosporine, a protein kinase inhibitor, resulted in a slightly upward curvature of the stolons (Fig. 1B). Increase of the staurosporine concentration to 5 and 10 μM further strengthened the curvature phenotype (Fig. 1A and B). Addition of 0.5 mM NaF, a protein phosphatase inhibitor, also led to upward bending of the stolons (Fig. 1B). Furthermore, the bending angle were enlarged as the concentration of NaF increased to 2.5 and 5 mM (Fig. 1A and B). Western blot analyses using pan-phosphorylation antibodies indicated that phosphorylation level of some proteins were up-

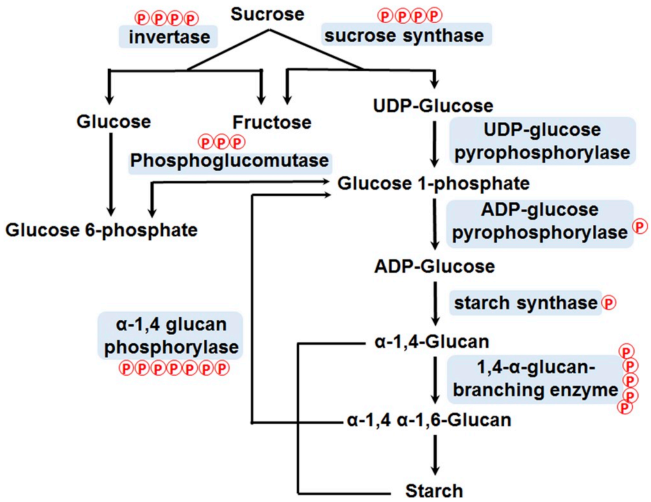

Fig. 4. Phosphoproteins involved in starch metabolism in bermudagrass stolons. Enzymes catalyzing each steps of the starch synthesis and degradation (except UDP-glucose pyrophosphorylate) were identified as phosphoproteins. Numbers of phosphorylation sites on each proteins were marked with red circle. . (For interpretation of the references to colour in this figure legend, the reader is referred to the Web version of this article.)

regulated and down-regulated under NaF and staurosporine treatment, respectively (Fig. S1). These observations collectively implied that reversible protein phosphorylation is important for gravitropism of bermudagrass stolons. Similar altered gravitropic response was also observed in oat shoot pulvini treated with staurosporine and NaF (Chang and Kaufman, 2000), suggesting a conserved phosphorylation-dependent regulatory module of gravitropism might exist in plants.

Except for altered gravitropic response, leaves growing out from the stolon nodes showed various degree of wilting symptoms under the two inhibitor treatments (Fig. 1A). I_2-KI staining indicated that massive starch were accumulated in stolon internodes of bermudagrass, however, the accumulation of starch was impaired under both staurosporine and NaF treatments (Fig. 1C). Similar rapid loss of starch was also observed in oat shoot pulvini under okadaic acid treatment (Chang et al., 2001). Accumulation of starch in the stolon internodes could provide necessitous carbohydrate nutrition to the new tillers and leaves growing out from the stolon nodes (Giolo et al., 2013; Thalmann and Santelia, 2017). On the other hand, water and mineral nutrition were continually transported from roots to leaves through vascular systems of stolons (Munshaw et al., 2001). The observed wilting of leaves and impeded accumulation of starch under inhibitor treatments strongly implied that reversible phosphorylation plays important regulatory roles in these important physiological processes of bermudagrass stolons.

3.2. Phosphopeptide identification from bermudagrass stolons

To better understand the functions of phosphorylation modifications, we used shot-gun MS/MS analyses to identify phosphoproteins in bermudagrass stolons. Conventionally, shot-gun MS/MS identification of phosphoproteins require to enrich phosphopeptides (Nakagami et al., 2012; Werth et al., 2017; Zhang et al., 2013, 2019). However, enrichment procedures using either TiO_2 or TMAC are highly selective and biased, resulting in loss of phosphopeptides not binding to the specific resins. In this study, we tried to directly identify phosphopeptides using high-resolution mass spectrometer without enrichment. Although this method might lead to a reduction of identified phosphopeptides, novel phosphopeptides which can't be identified using traditional enrichment method could be revealed. Following this scenario, 3, 177 proteins containing 10, 124 unique peptides were successfully identified from 190, 707 MS/MS spectra of the trypsin-digested stolon protein extracts (Table S1). Among the 10, 124 peptides, 692 different peptides were identified as phosphopeptides (Table S2). One phosphopeptide (peptide FADDKDLQS^{P}EWR of alpha-1,4 glucan phosphorylase L isozyme, chloroplastic/amyloplastic, protein accession no. PB.2333.21|m.169,462) with a relatively high PTM score (234.77) was represented as an example of the identification results (Fig. 2A).

Notably, 677 of the 692 phosphopeptides contained only one phosphorylated residues, whereas 12, 2 and 1 phosphopeptides contained two, three and four phosphorylated residues, respectively (Fig. 2B; Table S2). Because 55 phosphorylation sites repeatedly occurred in 116 phosphopeptides (Table S3), totally 646 nonredundant phosphorylation sites were finally identified. Among the 646 phosphorylation sites, 548, 96 and 2 were phosphorylated at serine, threonine and tyrosine residues, respectively (Fig. 2C). Moreover, 419 (65%) nonredundant phosphorylation sites were found to have been identified in other plants via BLAST searches against the dbPPT phosphopeptide

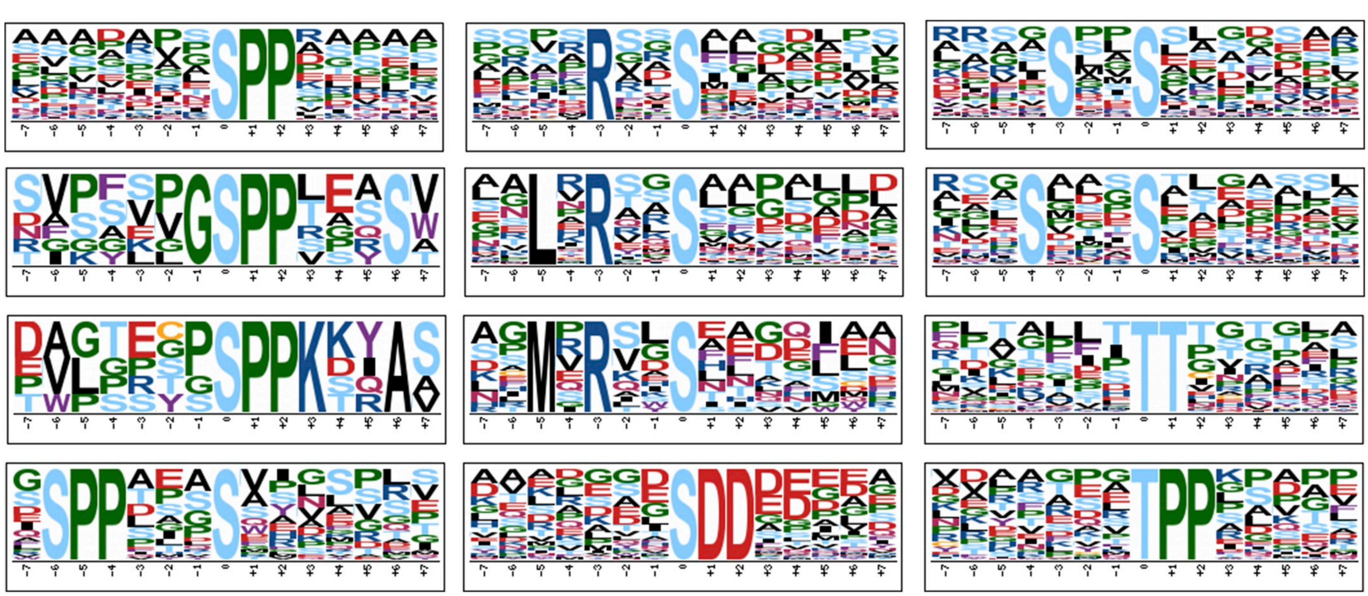

Fig. 5. Analyses of phosphorylation motifs in bermudagrass stolons. Motif-X analysis of the phosphopeptides was performed with a 15-amino acid window, a minimum occurrence of 20, and significance p-value of 10^{-6}.

database (Fig. 2D; Table S2), implying that the remaining 227 are new protein phosphorylation sites in plants. These results collectively indicated that shot-gun MS/MS analyses without enrichment could identify substantial and novel phosphopeptides.

3.3. Functional diversity of phosphoproteins in bermudagrass stolons

The 646 nonredundant phosphorylation sites of 692 phosphopeptides were mapped on 485 proteins (Table S2). Over three quarter of phosphoproteins were only phosphorylated at one residue, whereas 106 phosphoproteins were phosphorylated at two or more residues (Fig. 3A). Specifically, two proteins that are involved in carbohydrate metabolism, including alpha-1,4 glucan phosphorylase L isozyme, chloroplastic/amyloplastic (PB.2333.21|m.169,462) and monosaccharide-sensing protein 2 (PB.16,710.9|m.135,344), were both phosphorylated at more than five residues (Table S2). GO annotation indicated that the phosphoproteins belonged to 189 cellular components, performed 279 different molecular functions and participated in 1105 diverse biological processes (Table S4). These results are in line with the notion that phosphorylation regulate nearly all aspects of cellular activities.

Because the 485 phosphoproteins and 3, 177 total proteins were identified from the same stolon samples at the same time, we could use GO enrich analysis to estimate the molecular functions and biological processes that are significantly regulated by phosphorylation. The results indicated that eight molecular functions and 12 biological processes were significantly enriched with phosphoproteins (Fig. 3B and C). Specifically, as many as 30 protein kinases were identified as phosphoproteins, which makes the protein kinase activity and phosphorylation the most significantly enriched molecular function and biological process, respectively (Table 1; Fig. 3B and C). These results implied that phosphorylation regulation itself was also regulated by reversible phosphorylation in bermudagrass stolons.

Many biological processes, including sucrose metabolism, starch synthesis and degradation, regulation of pH, transmembrane transport of ions and other molecules, phototropism and negative gravitropism, which are important for starch accumulation and mobilization, maintaining high-efficient transport system, and prostrate growth of stolons, were all significantly regulated by phosphorylation (Fig. 3C). Interestingly, these processes were not assigned as significantly regulated GO categories in other phosphoproteomics studies, suggesting their unique and important physiological functions in bermudagrass stolons. Specifically, in accordance with previous findings that starch metabolism was regulated by protein phosphorylation (White-Gloria et al., 2018; Zhen et al., 2017), we found that enzymes involved in dynamic equilibrium of starch were all phosphorylated in bermudagrass stolons except UDP-glucose pyrophosphorylate (Fig. 4). These results partially explained why the starch content of bermudagrass stolons sharply decreased under kinase and phosphatase inhibitor treatments (Fig. 1C).

3.4. Conserved and novel phosphorylation motifs in bermudagrass stolons

The amino acids surrounding a phosphorylation site constitute specific recognition motifs for kinases and phosphatases (Al-Momani et al., 2018). Using Motif-X tool, we assessed the enrichment of motifs around the 646 nonredundant phosphorylation sites. Totally, 10 phosphoserine and two phosphothreonine motifs were successfully identified (Fig. 5). Among these motifs, two phosphoserine motifs, GS^{P}PPxxxS and S^{P}PPKxxA, were subtypes of S^{P}PP motif, whereas other two phosphoserine motifs, LxRxxS^{P} and MxRxxS^{P}, were subtypes of RxxS^{P} motif (Fig. 5). Phosphoproteins containing LxRxxS^{P} and MxRxxS^{P} motifs were reported to be possible substrates of AMPK kinases, whereas phosphoproteins containing RxxS^{P} motif without proximal leucine and methionine residues were possible substrates of PKAs or calcium/calmodulin-dependent protein kinases (van Wijk et al., 2014).

Serine or threonine residues preceding proline (S^{P}/T^{P}P) are the major regulatory phosphorylation motifs that function in diverse cellular processes (Lu et al., 2002). Previous phosphoproteomics studies all identified the conserved S^{P}P and T^{P}P motifs in diverse plant tissues (Gupta et al., 2018; Meyer et al., 2012; Vu et al., 2018; Wang et al., 2013; Yuan et al., 2016). In this study, we found that the two motifs were further specialized to novel S^{P}PP and T^{P}PP motifs with two proline residues in bermudagrass stolons. Interestingly, phosphoproteins that play important roles in transcription regulation, including far upstream element-binding protein 1 (PB.8693.3|m.19,754), zinc finger CCCH domain-containing protein 33 (PB.32,192.8|m.106,576), transcription factor BIM1-like (PB.16,199.13|m.130,259), histone deacetylase 2 isoform X2 (PB.58,701.4|m.57,109), apoptotic chromatin condensation inducer in the nucleus (PB.3346.9|m.140,044) and serine/arginine-rich splicing factor RSZ23-like (PB.63,673.2|m.43,347), were all phosphorylated at either one of the two novel motifs (Table S2). These results implied that specific kinases or phosphatases might play important regulatory roles in gene expression of bermudagrass stolons, through catalyzing the reversible phosphorylation of proteins containing the two novel motifs.

4. Conclusion

In this study, we found that reversible phosphorylation modification plays important roles in gravitropic response and starch accumulation of bermudagrass stolons. Through unbiased MS/MS analyses, totally 646 nonredundant phosphorylation sites of 485 phosphoproteins were successfully identified from 692 phosphopeptides. These phosphoproteins have diverse cellular and biochemical activities and were enriched in 12 biological processes. Two novel phosphorylation motifs, S^{P}PP and T^{P}PP were further identified from the phosphoproteins through Motif-X analyses. These results collectively expanded our understanding of bermudagrass stolons to a post-translational level.

Author contributions

B. Z. designed and conceived the research and wrote the manuscript. J. C., J. Z., X. Y., and J. L. participated in the experiments and helped to write the manuscript. All authors read and approved the final manuscript.

Acknowledgments

We are grateful to Wuhan GeneCreate Biological Engineering Corporation for the technical assistance in phosphopeptide identification. We want to thank the reviewers for providing constructive comments on the manuscript. This work was financially supported by the National Natural Science Foundation of China (31601786) and the Natural Science Foundation of Jiangsu Province (BK20160596).

Appendix A. Supplementary data

Supplementary data to this article can be found online at https://doi.org/10.1016/j.plaphy.2019.09.036.

References

Al-Momani, S., Qi, D., Ren, Z., Jones, A.R., 2018. Comparative qualitative phosphoproteomics analysis identifies shared phosphorylation motifs and associated biological processes in evolutionary divergent plants. J Proteomics 181, 152–159.

Balatti, P.A., Willemöes, J.G., 1989. Role of ethylene in the geotropic response of bermudagrass (*Cynodon dactylon* L. Pers.) stolons. Plant Physiol 91, 1251–1254.

Beltrano, J., Willemoes, J., Montaldi, E.R., Barreiro, R., 1991. Photoassimilate partitioning modulated by phytochrome in Bermuda grass (*Cynodon dactylon* (L) Pers.). Plant Sci. 73, 19–22.

Bradford, M.M., 1976. A rapid and sensitive method for the quantitation of microgram quantities of protein utilizing the principle of protein-dye binding. Anal. Biochem. 72, 248–254.

Carbon, S., Ireland, A., Mungall, C.J., Shu, S., Marshall, B., Lewis, S., AmiGO Hub; Web

Presence Working Group, 2009. AmiGO: online access to ontology and annotation data. Bioinformatics 25, 28–29.

Chang, S.C., Cho, M.H., Kang, B.G., Kaufman, P.B., 2001. Changes in starch content in oat (*Avena sativa*) shoot pulvini during the gravitropic response. J. Exp. Bot. 52, 1029–1040.

Chang, S.C., Kaufman, P.B., 2000. Effects of staurosporine, okadaic acid and sodium fluoride on protein phosphorylation in graviresponding oat shoot pulvini. Plant Physiol. Biochem. 38, 315–323.

Chao, Q., Gao, Z.F., Wang, Y.F., Li, Z., Huang, X.H., Wang, Y.C., Mei, Y.C., Zhao, B.G., Li, L., Jiang, Y.B., Wang, B.C., 2016. The proteome and phosphoproteome of maize pollen uncovers fertility candidate proteins. Plant Mol. Biol. 91, 287–304.

Chen, J., Jiang, Q., Zong, J., Chen, Y., Chu, X., Liu, J., 2014. Variation in the salt-tolerance of 13 genotypes of hybrid bermudagrass [*Cynodon dactylon* (L.) Pers. × *C. transvaalensis* Burtt-Davy] and its relationship with shoot Na^+, K^+, and Cl^- ion concentrations. J. Hortic. Sci. Biotechnol. 89, 35–40.

Chen, L., Fan, J., Hu, Z., Huang, X., Amombo, E., Liu, A., Bi, A., Chen, K., Xie, Y., Fu, J., 2017. Melatonin is involved in regulation of bermudagrass growth and development and response to low K^+ stress. Front. Plant Sci. 8, 2038.

Cheng, H., Deng, W., Wang, Y., Ren, J., Liu, Z., Xue, Y., 2014. dbPPT: a comprehensive database of protein phosphorylation in plants. Database 2014: bau121.

Clore, A.M., Turner, W.S., Morse, A.M., Whetten, R.W., 2003. Changes in mitogen-activated protein kinase activity occur in the maize pulvinus in response to gravistimulation and are important for the bending response. Plant Cell Environ. 26, 991–1001.

Dunne, J.C., Tuong, T.D., Livingston, D.P., Reynolds, W.C., Milla-Lewis, S.R., 2019. Field and laboratory evaluation of bermudagrass germplasm for cold hardiness and freezing tolerance. Crop Sci. 59, 392–399.

Fermin, D., Avtonomov, D., Choi, H., Nesvizhskii, A.I., 2015. LuciPHOr2: site localization of generic post-translational modifications from tandem mass spectrometry data. Bioinformatics 31, 1141–1143.

Giolo, M., Macolino, S., Barolo, E., Rimi, F., 2013. Stolons reserves and spring green-up of seeded bermudagrass cultivars in a transition zone environment. Hortscience 48, 780–784.

Guglielmini, A.C., Satorre, E.H., 2002. Shading effects on spatial growth and biomass partitioning of *Cynodon dactylon*. Weed Res. 42, 123–134.

Gupta, R., Min, C.W., Meng, Q., Agrawal, G.K., Rakwal, R., Kim, S.T., 2018. Comparative phosphoproteome analysis upon ethylene and abscisic acid treatment in *Glycine max* leaves. Plant Physiol. Biochem. 130, 173–180.

Kameyama, K., Kishi, Y., Yoshimura, M., Kanzawa, N., Sameshima, M., Tsuchiya, T., 2000. Tyrosine phosphorylation in plant bending. Nature 407, 37.

Li, L., Ljung, K., Breton, G., Schmitz, R.J., Pruneda-Paz, J., Cowing-Zitron, C., Cole, B.J., Ivans, L.J., Pedmale, U.V., Jung, H.S., Ecker, J.R., Kay, S.A., Chory, J., 2012. Linking photoreceptor excitation to changes in plant architecture. Genes Dev. 26, 785–790.

Liñeiro, E., Chiva, C., Cantoral, J.M., Sabido, E., Fernández-Acero, F.J., 2016. Phosphoproteome analysis of *B. cinerea* in response to different plant-based elicitors. J. Proteomics 139, 84–94.

Lu, K.P., Liou, Y.C., Zhou, X.Z., 2002. Pinning down proline-directed phosphorylation signaling. Trends Cell Biol. 12, 164–172.

Lu, T.C., Meng, L.B., Yang, C.P., Liu, G.F., Liu, G.J., Ma, W., Wang, B.C., 2008. A shotgun phosphoproteomics analysis of embryos in germinated maize seeds. Planta 228, 1029–1041.

Lulli, F., Guglielminetti, L., Grossi, N., Armeni, R., Stefanini, S., Volterrani, M., 2011. Physiological and morphological factors influencing leaf, rhizome and stolon tensile strength in C4 turfgrass species. Funct. Plant Biol. 38, 919–926.

Lv, D.W., Subburaj, S., Cao, M., Yan, X., Li, X., Appels, R., Sun, D.F., Ma, W., Yan, Y.M., 2014. Proteome and phosphoproteome characterization reveals new response and defense mechanisms of *Brachypodium distachyon* leaves under salt stress. Mol. Cell. Proteom. 13, 632–652.

Meyer, L.J., Gao, J., Xu, D., Thelen, J.J., 2012. Phosphoproteomic analysis of seed maturation in Arabidopsis, rapeseed, and soybean. Plant Physiol. 159, 517–528.

Montaldi, E.R., 1969. Gibberellin-sugar interaction regulating the growth habit of bermudagrass (*Cynodon dactylon* (L) Pers). Cell. Mol. Life Sci. 25, 91–92.

Munshaw, G.C., Williams, D.W., Cornelius, P.L., 2001. Management strategies during the establishment year enhance production and fitness of seeded bermudagrass stolons. Crop Sci. 41, 1558–1564.

Munshaw, G.C., Zhang, X., Ervin, E.H., 2004. Effect of salinity on bermudagrass cold hardiness. Hortscience 39, 420–423.

Nakagami, H., Sugiyama, N., Ishihama, Y., Shirasu, K., 2012. Shotguns in the front line: phosphoproteomics in plants. Plant Cell Physiol. 53, 118–124.

Nakagami, H., Sugiyama, N., Mochida, K., Daudi, A., Yoshida, Y., Toyoda, T., Tomita, M., Ishihama, Y., Shirasu, K., 2010. Large-scale comparative phosphoproteomics identifies conserved phosphorylation sites in plants. Plant Physiol 153, 1161–1174.

Needham, E.J., Parker, B.L., Burykin, T., James, D.E., Humphrey, S.J., 2019. Illuminating the dark phosphoproteome. Sci. Signal. 12, eaau8645.

Pan, D., Wang, L., Tan, F., Lu, S., Lv, X., Zaynab, M., Cheng, C.L., Abubakar, Y.S., Chen, S., Chen, W., 2018. Phosphoproteomics unveils stable energy supply as key to flooding tolerance in *Kandelia candel*. J Proteomics 176, 1–12.

Rose, C.M., Venkateshwaran, M., Volkening, J.D., Grimsrud, P.A., Maeda, J., Bailey, D.J., Park, K., Howes-Podoll, M., den Os, D., Yeun, L.H., Westphall, M.S., Sussman, M.R., Ané, J.M., Coon, J.J., 2012. Rapid phosphoproteomic and transcriptomic changes in the rhizobia-legume symbiosis. Mol. Cell. Proteom. 11, 724–744.

Schwartz, D., Gygi, S.P., 2005. An iterative statistical approach to the identification of protein phosphorylation motifs from large-scale data sets. Nat. Biotechnol. 23, 1391–1398.

Silva-Sanchez, C., Li, H., Chen, S., 2015. Recent advances and challenges in plant phosphoproteomics. Proteomics 15, 1127–1141.

Thalmann, M., Santelia, D., 2017. Starch as a determinant of plant fitness under abiotic stress. New Phytol. 214, 943–951.

Tyanova, S., Temu, T., Cox, J., 2016. The MaxQuant computational platform for mass spectrometry-based shotgun proteomics. Nat. Protoc. 11, 2301–2319.

van Wijk, K.J., Friso, G., Walther, D., Schulze, W.X., 2014. Meta-analysis of *Arabidopsis thaliana* phospho-proteomics data reveals compartmentalization of phosphorylation motifs. Plant Cell 26, 2367–2389.

Vannini, C., Marsoni, M., Scoccianti, V., Ceccarini, C., Domingo, G., Bracale, M., Crinelli, R., 2019. Proteasome-mediated remodeling of the proteome and phosphoproteome during kiwifruit pollen germination. J Proteomics 192, 334–345.

Vu, L.D., Zhu, T., Verstraeten, I., van de Cotte, B., International Wheat Genome Sequencing Consortium, Gevaert, K., De Smet, I., 2018. Temperature-induced changes in the wheat phosphoproteome reveal temperature-regulated interconversion of phosphoforms. J. Exp. Bot. 69, 4609–4624.

Wang, F., Smith, A.G., Brenner, M.L., 1994. Temporal and spatial expression pattern of sucrose synthase during tomato fruit development. Plant Physiol 104, 535–540.

Wang, J., Yu, L., Huang, X., Wang, Y., Zhao, J., 2016. Comparative proteome analysis of saccular intracranial aneurysms with iTRAQ quantitative proteomics. J Proteomics 130, 120–128.

Wang, X., Bian, Y., Cheng, K., Gu, L.F., Ye, M., Zou, H., Sun, S.S., He, J.X., 2013. A large-scale protein phosphorylation analysis reveals novel phosphorylation motifs and phosphoregulatory networks in Arabidopsis. J Proteomics 78, 486–498.

Werth, E.G., McConnell, E.W., Gilbert, T.S., Couso Lianez, I., Perez, C.A., Manley, C.K., Graves, L.M., Umen, J.G., Hicks, L.M., 2017. Probing the global kinome and phosphoproteome in *Chlamydomonas reinhardtii* via sequential enrichment and quantitative proteomics. Plant J. 89, 416–426.

White-Gloria, C., Johnson, J.J., Marritt, K., Kataya, A., Vahab, A., Moorhead, G.B., 2018. Protein kinases and phosphatases of the plastid and their potential role in starch metabolism. Front. Plant Sci. 9, 1032.

Willemoës, J.G., Beltrano, J., Montaldi, E.R., 1987. Stolon differentiation in *Cynodon dactylon* (L.) Pers. mediated by phytochrome. Environ. Exp. Bot. 27, 15–20.

Wu, J., Wang, B., Xin, X., Ren, D., 2018. Protein kinases in shaping plant architecture. Curr. Protein Pept. Sci. 19, 390–400.

Yao, Y., Yang, Y.W., Liu, J.Y., 2006. An efficient protein preparation for proteomic analysis of developing cotton fibers by 2-DE. Electrophoresis 27, 4559–4569.

Yuan, L.L., Zhang, M., Yan, X., Bian, Y.W., Zhen, S.M., Yan, Y.M., 2016. Dynamic phosphoproteome analysis of seedling leaves in *Brachypodium Distachyon* L. reveals central phosphorylated proteins involved in the drought stress response. Sci. Rep. 6, 35280.

Zhang, B., Liu, J., 2018. Molecular cloning and sequence variance analysis of the *TEOSINTE BRANCHED1* (*TB1*) gene in bermudagrass [*Cynodon dactylon* (L.) Pers]. J. Plant Physiol. 229, 142–150.

Zhang, B., Liu, J., Wang, X., Wei, Z., 2018. Full-length RNA sequencing reveals unique transcriptome composition in bermudagrass. Plant Physiol. Biochem. 132, 95–103.

Zhang, B., Xiao, X., Zong, J., Chen, J., Li, J., Guo, H., Liu, J., 2017. Comparative transcriptome analysis provides new insights into erect and prostrate growth in bermudagrass (*Cynodon dactylon* L.). Plant Physiol. Biochem. 121, 31–37.

Zhang, H., Zhou, H., Berke, L., Heck, A.J., Mohammed, S., Scheres, B., Menke, F.L., 2013. Quantitative phosphoproteomics after auxin-stimulated lateral root induction identifies an SNX1 protein phosphorylation site required for growth. Mol. Cell. Proteom. 12, 1158–1169.

Zhang, M., Lv, D., Ge, P., Bian, Y., Chen, G., Zhu, G., Li, X., Yan, Y., 2014. Phosphoproteome analysis reveals new drought response and defense mechanisms of seedling leaves in bread wheat (*Triticum aestivum* L.). J Proteomics 109, 290–308.

Zhang, Z., Ke, D., Hu, M., Zhang, C., Deng, L., Li, Y., Li, J., Zhao, H., Cheng, L., Wang, L., Yuan, H., 2019. Quantitative phosphoproteomic analyses provide evidence for extensive phosphorylation of regulatory proteins in the rhizobia-legume symbiosis. Plant Mol. Biol. 100, 265–283.

Zhao, Q., Chen, W., Bian, J., Xie, H., Li, Y., Xu, C., Ma, J., Guo, S., Chen, J., Cai, X., Wang, X., Wang, Q., She, Y., Chen, S., Zhou, Z., Dai, S., 2018. Proteomics and phosphoproteomics of heat stress-responsive mechanisms in spinach. Front. Plant Sci. 9, 800.

Zhen, S., Deng, X., Zhang, M., Zhu, G., Lv, D., Wang, Y., Zhu, D., Yan, Y., 2017. Comparative phosphoproteomic analysis under high-nitrogen fertilizer reveals central phosphoproteins promoting wheat grain starch and protein synthesis. Front. Plant Sci. 8, 67.